DEVELOPMENT OF DIAGNOSTICS AND DATA ANALYSIS ON ASDEX IN 1989[1)]

IPP III / 158

JUNE 1990

MAX-PLANCK-INSTITUT FÜR PLASMAPHYSIK

8046 GARCHING BEI MÜNCHEN

MAX-PLANCK-INSTITUT FÜR PLASMAPHYSIK

GARCHING BEI MÜNCHEN

DEVELOPMENT OF DIAGNOSTICS AND DATA ANALYSIS ON ASDEX IN 1989[1)]

IPP III / 158 JUNE 1990

[1)] This report has originally been written for the Annual Report 1989, chapter 2.0

Die nachstehende Arbeit wurde im Rahmen des Vertrages zwischen dem Max-Planck-Institut für Plasmaphysik und der Europäischen Atomgemeinschaft über die Zusammenarbeit auf dem Gebiete der Plasmaphysik durchgeführt.

DEVELOPMENT OF DIAGNOSTICS AND DATA ANALYSIS ON ASDEX IN 1989

CONTENTS

2.1 Broadband Microwave Reflectometry

(M.E. Manso, F. Serra, A. Silva, J. Matias, F. Nunes (Instituto Superior Tecnico, Lisboa, Portugal), J. Neves, J. Pereira (Universidade de Aveiro, Aveiro, Portugal), G. Siller, F.X. Söldner)

The ASDEX reflectometric system had started swept-frequency operation by mid-December 1988. Data analysis and processing was routinely carried out during the measuring campaign of April - August 1989, allowing density profiles to be obtained; the first plasma physics studies, based on the obtained experimental results, have been done. Preliminary measurements in fixed-frequency operation were obtained in August 1989, with homodynic detection (K and K_a bands).

During the summer shutdown of ASDEX, several modifications were made to the reflectometric system: (1) the existing homodynic detection was improved, (2) a very sensitive heterodynic detection was developed, and (3) the system was upgraded by installing three new reflectometers. A new measuring campaign began in November 1989, when ASDEX operation was resumed. Commissioning of the new detection system is envisaged for February 1990 and will allow sensitive measurement of plasma density fluctuations.

Microwave reflectometry is based on the propagation and reflection of a probing wave (F) in an inhomogeneous plasma. Two modes of operation (O and X) are possible. In the O-mode, the reflection condition (cut-off) depends only on the local plasma density $n_e(r)$; in the X-mode it depends on both the plasma density and the value of the local magnetic field. In the O-mode the density of a reflecting plasma layer $n_e(X_c)$ is determined by the microwave frequency (F); the position X_c is evaluated from the phase delay $\phi(F)$ between the incident and reflected waves. If the frequency is swept, a density profile can be obtained from the phase shift $\Delta\phi/\Delta f$ the wave undergoes in the plasma, integrated from f = 0 to f = F:

$$X_c(F) = \int_0^F \left(\frac{d\phi}{df}\right) df \,/\, \sqrt{F^2 - f^2} \quad ;$$

in fixed-frequency operation, movements of the reflecting layer can be detected.

The ASDEX reflectometric system consists of three reflectometers in the frequency bands 18 - 26.5 GHz (K band), 26.5 - 40 GHz (K_a band) and 40 - 60 GHz (U band). Thus, electron densities from $4 \cdot 10^{12}$ cm^{-3} to $4.45 \cdot 10^{13}$ cm^{-3} can be probed (O-mode). Broadband measurements are made with simultaneous swept operation of the three reflectometers, allowing a density profile measurement during 2 ms. The diagnostic has a control and data acquisition system based on standard Camac modules controlled by a PC-AT computer. The system allows a maximum of ~100 profiles to be obtained per shot with a ~3 ms interval between every two sweeps. Typical spatial resolutions of the density profiles measurements are 1 - 1.5 cm in the scrape-off layer and 2 - 2.5 cm in the gradient region.

The diagnostic is specially suited to performing measurements in the gradient region, starting from the plasma radius close to the magnetic separatrix (where $n_e \lesssim 1 \cdot 10^{13}$ cm^{-3}). The O-mode was chosen in view of its advantages for profile measurements: (a) the cut-off depends only on the plasma density, and so measurements are not limited to certain values of the toroidal magnetic field; (b) evaluation of a profile is quite simple (the phase integral can be analytically inverted) and requires little computing time; (c) profile measurements are less affected by density fluctuations than with the X-mode. However, the O-mode is not adequate for performing measurements below $4 \cdot 10^{12}$ cm^{-3}, and so for the most outer part of the profile the X-mode must be used.

As an example of typical broadband reflectometric measurements, we show in Fig. 1 signals obtained (a) during shot 27328 (ohmic, $\overline{n}_e = 3.9 \cdot 10^{13}$ cm^{-3}) and (b) before the plasma discharge. Clear fringes due to the plasma can be observed. The frequency minima, automatically detected, are indicated below the horizontal axis of the figure. The phase shift $\Delta\phi/\Delta f$ is evaluated from the minima for each frequency band and fitted to a unique curve as shown in Fig. 2a. The curve exhibits oscillations that result from the phase modulations of the reflectometric signals induced by the plasma density fluctuations. The experimental results show that the fluctuations have a greater effect on the evaluation of the steeper density gradients profiles, $dn_e / dX \gtrsim 0.2 \cdot 10^{13}$ cm^{-4}. Numerical studies are being conducted to correlate the measured $\Delta\phi/\Delta f$ oscillations with both the amplitude and frequency of the plasma density fluctuations.

Several numerical analysis techniques were developed in order to filter the perturbations. Figure 2b shows the phase shift curve of Fig. 2a after numerical filtering. The density profile evaluated from raw data is pre-

sented in Fig. 3. The profile was measured between the minor radii 43 cm and 8 cm. For r < 8 cm the reflected signals decrease, and their amplitudes become of the order of the noise level. The decrease can be due both to the flatness of the profile (shown by YAG and HCN data) and to the low sensitivity of the detectors for the highest frequencies of the U band. The

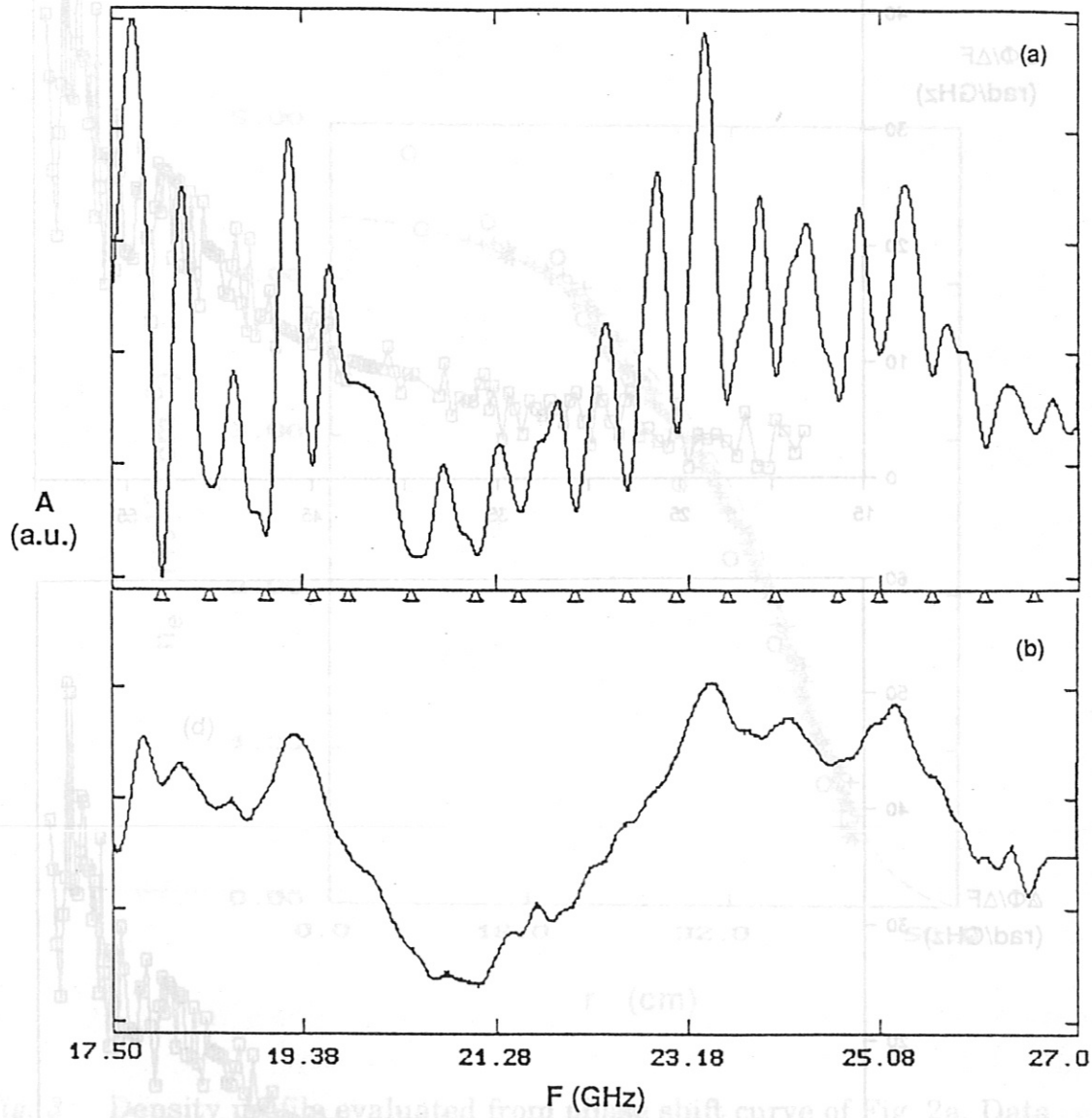

Fig. 1: Output signal of the K band reflectometer, ~17.5 - 27 GHz, obtained (a) during ASDEX shot 27328, in the time interval 1100 - 1102 ms, and (b) before the plasma discharge. Fringes due to the plasma can be clearly observed in (a).

Fig. 2

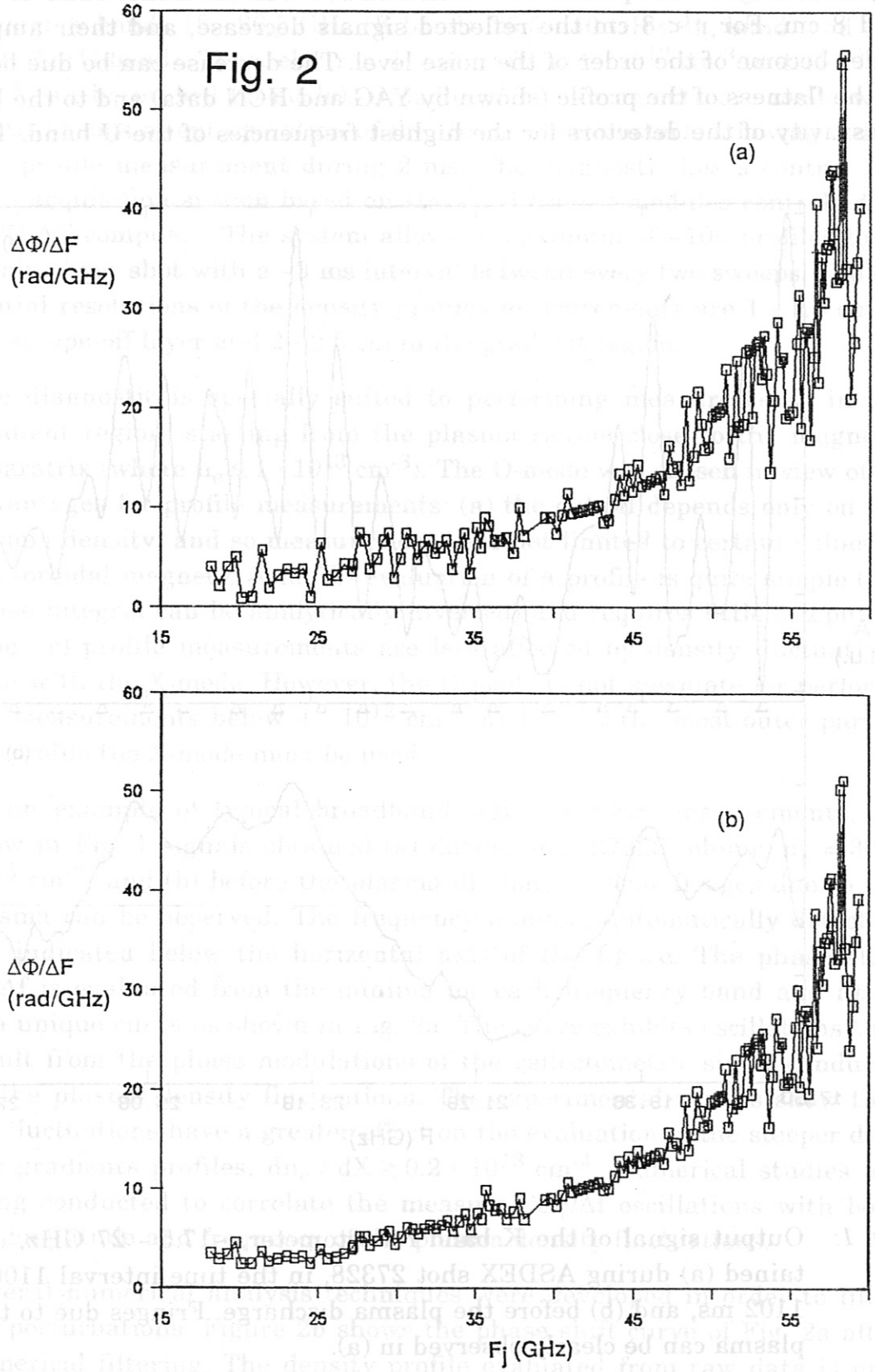

Fig. 2: Phase shift curves $\Delta\phi/\Delta f$ for the frequency range ~18 - 60 GHz, including the phase information from the three reflectometers, for shot 27328 (same time interval as in Fig. 1). Curve (a) corresponds to the minima (F_j) obtained from raw data, and (b) corresponds to the minima obtained from the smoothed phase ($\phi(F)$) characteristic.

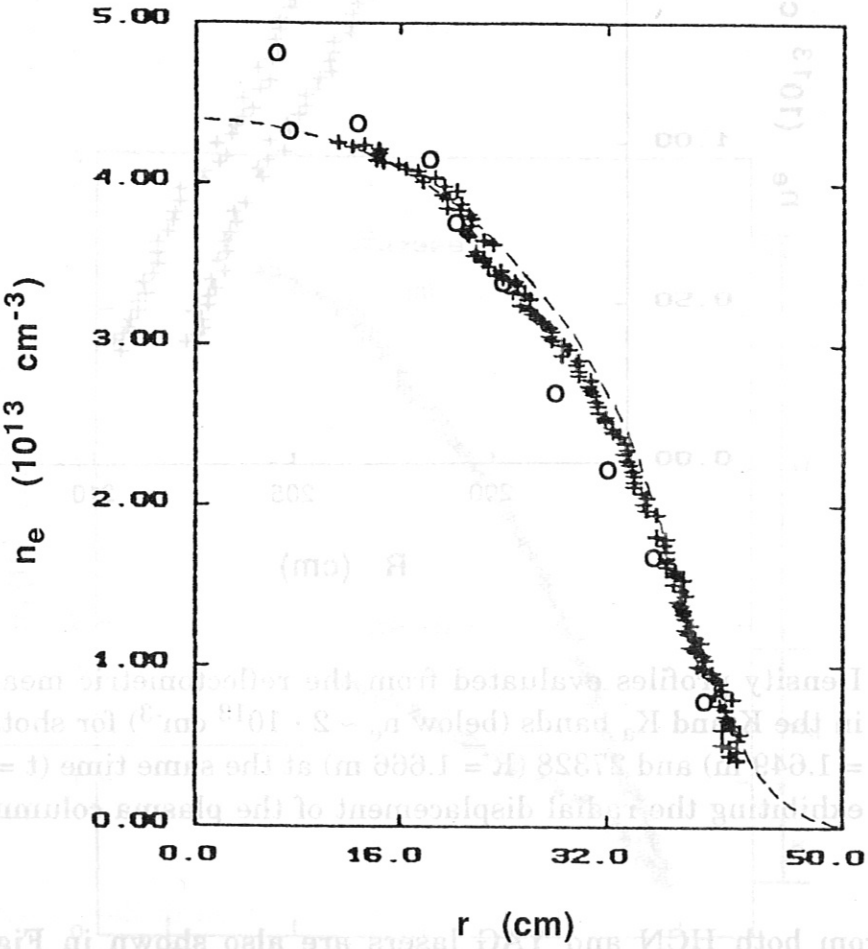

Fig. 3: Density profile evaluated from phase shift curve of Fig. 2a. Data from HCN interferometer (- - -) and YAG laser (O) are also shown.

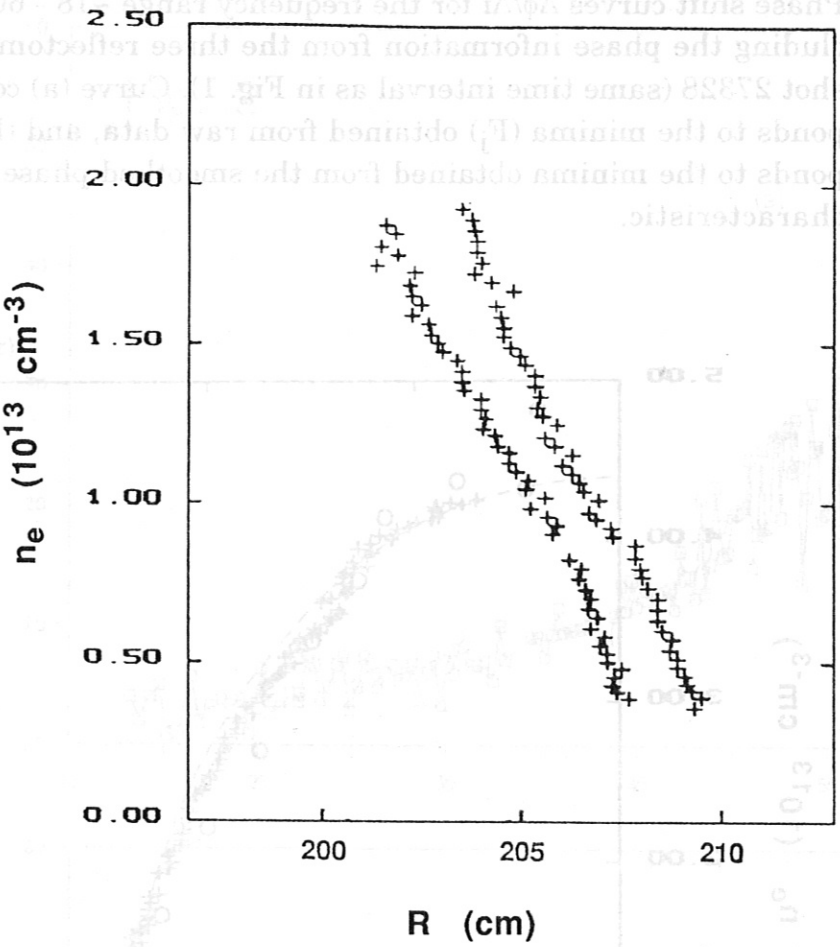

Fig. 4: Density profiles evaluated from the reflectometric measurements in the K and K_a bands (below $n_e \sim 2 \cdot 10^{13}$ cm^{-3}) for shots 27327 (R = 1.649 m) and 27328 (R = 1.666 m) at the same time (t = 1300 ms), exhibiting the radial displacement of the plasma column.

data from both HCN and YAG lasers are also shown in Fig. 3, these agreeing with the data from microwave reflectometry.

There is some uncertainty in the measurement of the profile in the scrape-off layer region owing to the fact that the phase shift $\Delta\phi/\Delta f$ cannot be measured for $f < F_1$ ~18 GHz, and a profile shape between X_o ($n_e = 0$) and the first reflecting layer X_1 has to be assumed. In the density profile shown above, a linear profile was considered. In order to check the validity of the linear shape, two similar shots, 27327 and 27328 (with the plasma radially displaced by 1.7 cm), were analyzed. The peripheral part

of the density profiles for $n_e \leq 2 \cdot 10^{13}$ cm^{-3} is presented in Fig. 4. A radial shift of ~1.7 cm between the two profiles is observed. It can therefore be concluded that, from the point of view of the profile evaluation, the linear profile is a good approximation in this case. Other shapes were considered and the study showed that only the outer part of the evaluated density profile ($\Delta X \sim 1$ cm) is sensitive to the non-measured part of the pedestal. The study was also done for low-density plasmas, $\bar{n}_e < 2.5 \cdot 10^{13}$ cm^{-3}, where no significant deviations were observed.

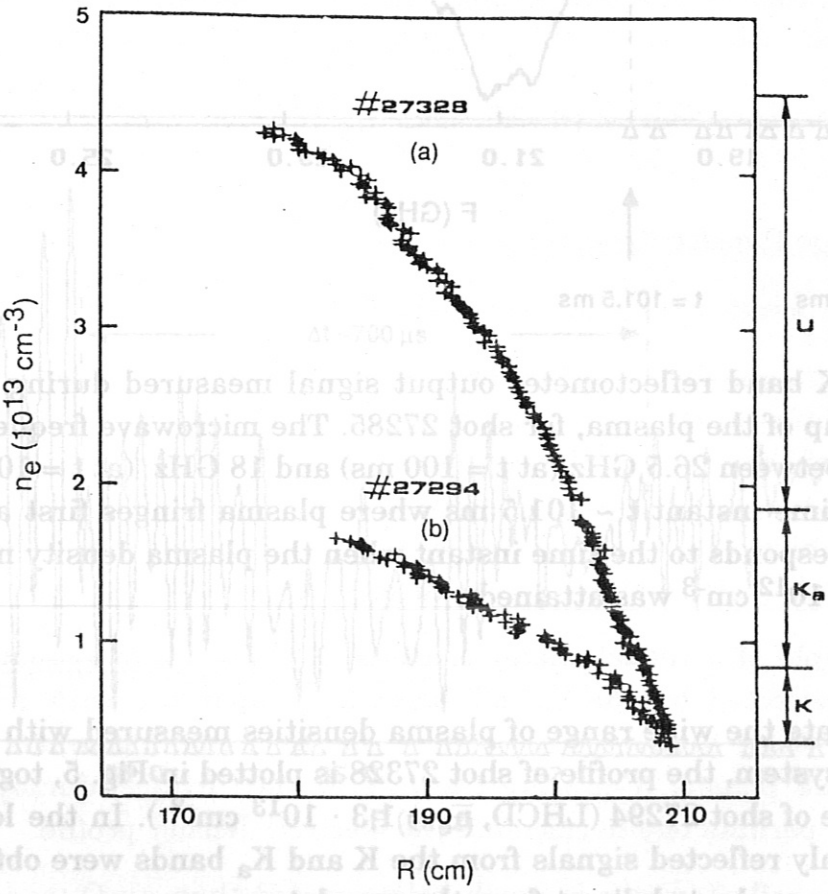

Fig. 5: Density profiles evaluated from reflectometric measurements for (a) the high-density plasma of shot 27328, $\bar{n}_e = 3.9 \cdot 10^{13}$ cm^{-3}, t = 1100 ms, obtained from the phase shift curve of Fig. 2b; (b) low-density plasma of shot 27294, $\bar{n}_e = 1.3 \cdot 10^{13}$ cm^{-3}, t = 1100 ms, obtained direct from the raw-data frequency minima.

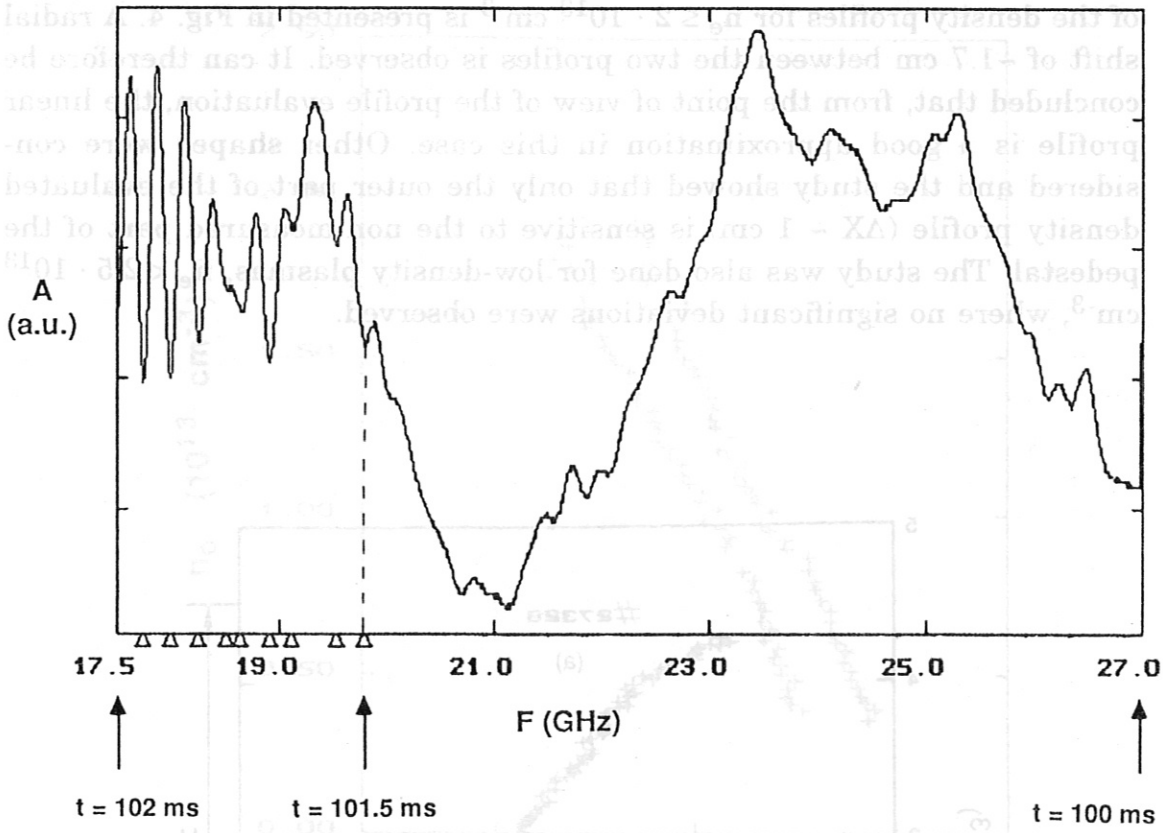

Fig. 6: K band reflectometer output signal measured during the ramp-up of the plasma, for shot 27285. The microwave frequency varies between 26.5 GHz (at t = 100 ms) and 18 GHz (at t = 102 ms). The time instant t ~ 101.5 ms where plasma fringes first appear corresponds to the time instant when the plasma density $n_e(0) \sim 4.88 \cdot 10^{12}$ cm^{-3} was attained.

To illustrate the wide range of plasma densities measured with the reflectometric system, the profile of shot 27328 is plotted in Fig. 5, together with the profile of shot 27294 (LHCD, $\overline{n}_e = 1.3 \cdot 10^{13}$ cm^{-3}). In the low-density plasma only reflected signals from the K and K_a bands were obtained; the profile was evaluated direct from the raw data.

Measurement of the time instants when significant modifications of the plasma-reflected wave occur provides relevant information about the temporal evolution of a profile, within the 2 ms measuring time. Two examples are presented in Figs. 6 and 7. The first one (Fig. 6) shows the output signal of the K band reflectometer, obtained during the ramp-up phase of shot 27285. Fringes are only observed for probing waves f < 19.9

GHz. As the highest-density layers are probed first (the oscillator is swept down), the time instant $t_1 \sim 101.5$ ms, when the fringes first appear, gives an estimate of the instant when the plasma has reached the value $n_e = 4.88 \cdot 10^{12}$ cm^{-3} ~ $n_e(0)$; the value obtained from the 6th channel of the YAG laser at t = 102 ms is ~$6 \cdot 10^{12}$ cm^{-3}. The second example is presented in Fig. 7, concerning shot 29285 when an m=2 tearing mode is present. The output signal of the K_a band reflectometer shows an abrupt decrease in both amplitude and (beat) frequency for densities $n_e(f)$ between 1.31 and $1.74 \cdot 10^{13}$ cm^{-3}, revealing a sudden increase in plasma density for these ranges. The signal modification is due to the rotating m=2 mode (f = 1.4 kHz) (see IPP Annual Report 1989, Sect. 1.8.2). From the time interval $\Delta t = (t_2 - t_1) \approx 700$ μs, when the perturbation was present, the value of the mode

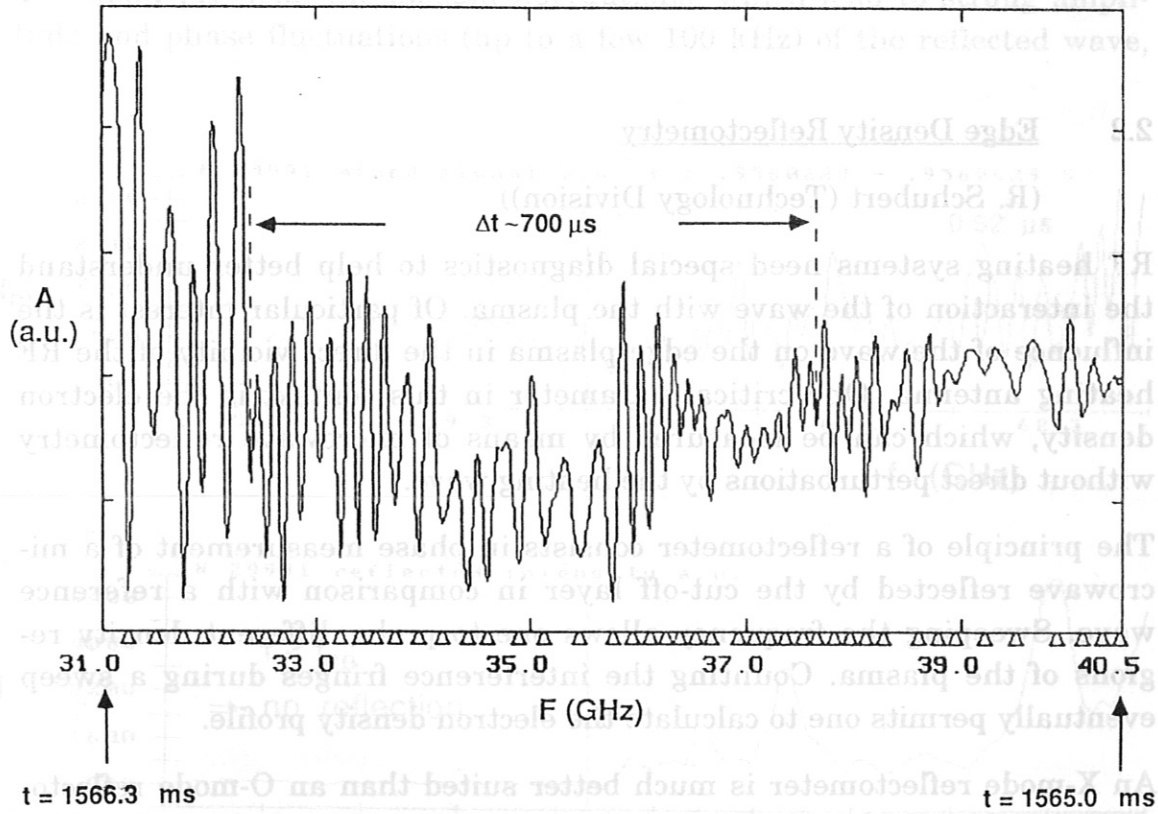

Fig. 7: Output signal of K_a band reflectometer, from t = 1565 ms to 1566.3 ms, for shot 29285, when a rotating magnetic island (f_{rot} ~ 1.4 kHz) is present. From the time interval $\Delta t \sim 700$ μs, the rotation frequency of ~1.4 kHz is obtained, in agreement with Mirnov probe data.

frequency can be determined: $f_{rot} = \Delta t^{-1} \approx 1.4$ kHz, in agreement with the magnetic data. Broadband reflectometry can therefore give the time scale of localized modifications of the profile, during the time interval of the measurement.

The main difficulty of profile evaluation comes from the errors in the phase shift resulting from the plasma density fluctuations. A detailed study of the $\Delta\phi/\Delta f$ characteristic for several plasma scenarios has been done and typical shapes for the different regimes were identified. This study served as a basis for developing nonlinear stochastic numerical filters (now being tested) that use a priori information of the phase, and that may provide a useful tool for routine evaluation of the data, even in situations where reflectometric signals are strongly disturbed by the plasma fluctuations.

2.2 Edge Density Reflectometry

(R. Schubert (Technology Division))

RF heating systems need special diagnostics to help better understand the interaction of the wave with the plasma. Of particular interest is the influence of the wave on the edge plasma in the direct vicinity of the RF heating antenna. One critical parameter in this context is the electron density, which can be measured by means of microwave reflectometry without direct perturbations by the heating wave.

The principle of a reflectometer consists in phase measurement of a microwave reflected by the cut-off layer in comparison with a reference wave. Sweeping the frequency allows one to probe different density regions of the plasma. Counting the interference fringes during a sweep eventually permits one to calculate the electron density profile.

An X-mode reflectometer is much better suited than an O-mode reflectometer, as described in Sect. 2.1, to these questions. (The very low densities in this region call for a very low frequency in the O-mode, which would give a very low spatial resolution. The antennas needed for the lower frequencies in the O-mode are too big.) Consequently, a completely independent reflectometer system was developed in the technology division.

The main features of the system are:

— X-mode (E perpendicular to B)
— the microwave frequency is swept from 60 to 80 GHz in 150 μs
— one sweep every 2.5 ms
— 2 antenna systems of the following dimensions are installed: (a) in a diagnostic hole in the Faraday screen of the NW-ICRF antenna: (1.9×3.8) mm^2 and (8×10) mm^2, (b) near the LH-grill: (8×10) mm^2 and (16×10) mm^2
— data acquisition: 10 MHz, 12 bit, 16 channels , 1 Mword each. This allows to acquire 160 sweeps per shot.

Depending on the plasma parameters, the system now in operation can measure the ranges $n_e < 10^{11}$ cm^{-3} to $n_e = 1.5 \cdot 10^{13}$ cm^{-3} and 1.95 m $\leq R \leq$ 2.15 m if B_t on axis is 2.8 T.

The main problem, the plasma fluctuations, which lead to strong amplitude and phase fluctuations (up to a few 100 kHz) of the reflected wave,

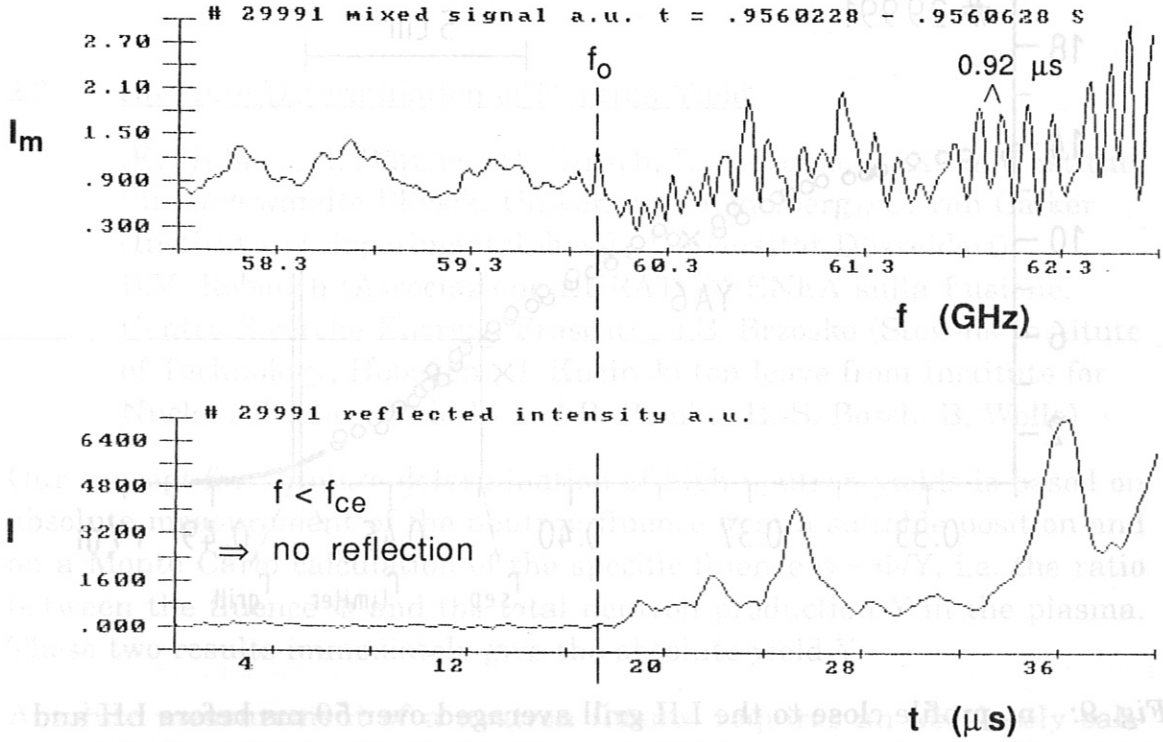

Fig. 8: First 40 μs of a sweep. The mixed signal I_m and the intensity I are simultaneously digitized. It is clearly seen that reflection begins at $f_o = f_{ce}$ at the antenna mouth.

could only be overcome by a very fast sweep in conjunction with a powerful digitizing system. This very fast sweep gives a fringe frequency of more than 1 MHz, so that the fringes cannot be blurred out by the fluctuations.

First profiles were obtained in June with the microwave antennas in the NW-ICRF antenna. In the summer break the system was upgraded and a second microwave antenna set was installed close to the LH grill, where first profiles were measured in December (see Fig. 9). Now the two systems are operational. It is also possible to use them in parallel, so that we can measure electron density profiles simultaneously at two different toroidal locations.

Figure 8 shows the first part of a sweep. The intensities of the reflected signal and the mixed signal (reflected and reference signals) are separately digitized. The following points are to be noted:

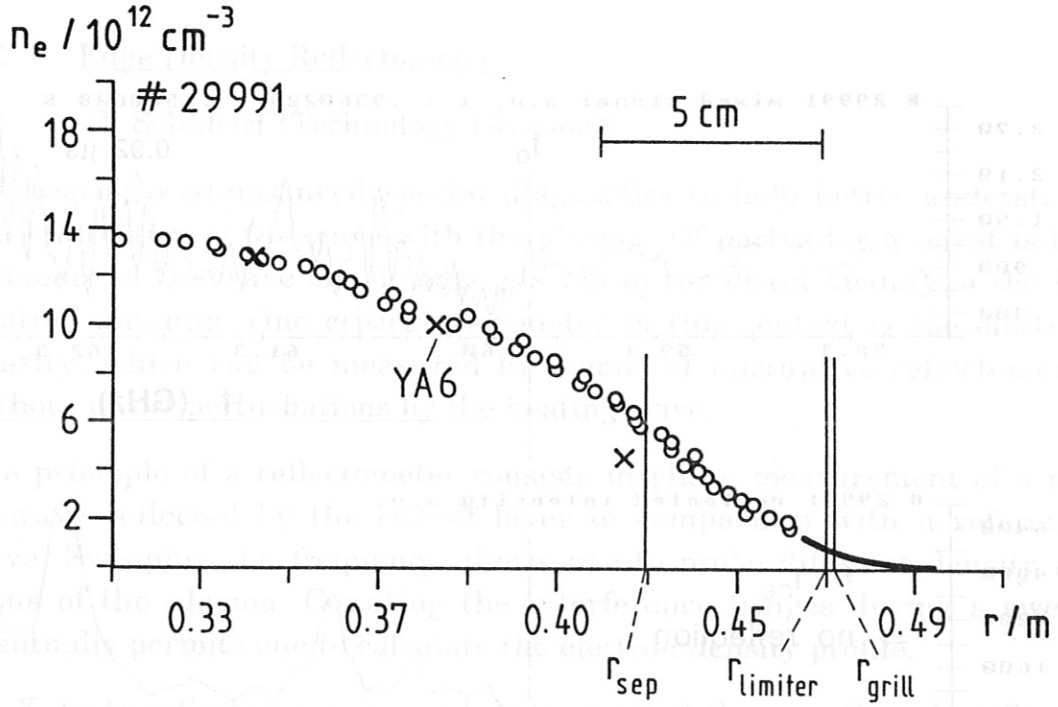

Fig. 9: n_e profile close to the LH grill averaged over 50 ms before LH and 50 ms after onset of LH. (n_e = 15 fringes, B_t = 2.8 T, YAG data (marked ×) are given for the OH case).

— Owing to the use of the X-mode, reflection does not begin till $f = f_0$ ($= f_{ce}$ at the antenna mouth), thus giving the location of the first reflection point. Hence, the absolute density profile can be calculated completely independently of any other diagnostic.
— The reflected intensity is strongly modulated in amplitude (factor of 10 and more, $f > 100$ kHz are present).
— The fringes appear at $f > 1$ MHz and are thus not perturbed by the fluctuations.

(The modulation in the first curve for $f < f_0$ is due to the frequency dependence of the microwave generator (BWO).)

Figure 9 shows the measured density of one of the first shots we made in connection with LH. The two profiles are obtained by averaging the phase over about 20 sweeps (50 ms). This averaging is necessary because the phase information we get out of one single sweep reflects the momentary profile, perturbed by the fluctuations, and not a stationary one.

2.3 Absolute Determination of Neutron Yield

(K. Hübner, R. Bätzner, H. Hinsch, L. Ingrosso, R. Klein (Institut für Angewandte Physik, Universität Heidelberg), C. van Calker (Institut für Experimentalphysik, Universität Düsseldorf), B.V. Robouch (Associazione EURATOM-ENEA sulla Fusione, Centro Ricerche Energie, Frascati), J.S. Brzosko (Stevens Institute of Technology, Hoboken), J. Kucinski (on leave from Institute for Nuclear Studies, Swierk) and B. Bomba, H.-S. Bosch, B. Wolle)

Our concept for absolute determination of high neutron yields is based on absolute measurement of the neutron fluence Φ at a suitable position and on a Monte Carlo calculation of the specific fluence $\varphi = \Phi/Y$, i.e. the ratio between the fluence Φ and the total neutron production Y in the plasma. These two results immediately give the absolute yield Y.

Absolute measurement of a neutron fluence requires an absolutely calibrated detector and unfolding of the response of the detector or an additional Monte Carlo simulation of its response to the specific fluence φ. We are using nuclear emulsions and indium activation; though the treat-

ment of emulsions is very time-consuming, they enable us to restrict the procedure to an appropriate interval of the neutron energy spectrum.

Monte Carlo calculation of the specific fluence φ is started from the spectral local neutron birth rate, which is determined by means of our neutron rate interpretation code from the measured plasma data for the discharges used for calibration. Starting from this plasma neutron source, the VINIA-3DAMC software is used to follow migration and scattering of neutrons through the full tokamak device and to determine the specific neutron fluence arriving in the detector.

In the past we have used at ASDEX a sequence of different positions with stepwise improvement of the ASDEX model, the software and the evaluation of the results. These results for Y are to be compared with the yields Y_c delivered from the counter array which is independently calibrated by using a neutron source in situ and scaling up to high neutron rates by successive plasma discharges with increasing yields.

For all nuclear emulsion measurements the results for the ratio Y/Y_c are between 1.0 and 1.2, with an error of the order of 30%. Thus, within the error bars we get excellent agreement between the two methods. The results for indium activation suffers essentially from the fact that we have to use here the full energy range between 0.3 and 3 MeV in the Monte Carlo simulation. For the calculations we have done so far, the error in the activation is of the order of 30%. Furthermore, absolute calibration of the measuring system is still under way. Nevertheless, the first result was $Y/Y_c = 0.9 - 1.4$; but this is now going to be essentially improved.

2.4 Ion Temperatures Deduced from Doppler Broadening of X-ray Lines

(Ch.-Ch. Chu (Experimental Plasma Physics Division 1))

Ion temperatures in ASDEX plasmas are obtained by measuring the full half-width of resonance line profiles of highly ionized elements in the soft X-ray range, 1 - 10 Å. A Johann spectrometer with a proportional counter is used to measure the emission of the resonance lines. The inclined line of sight covers a radial range from r = -32 cm to r = 8 cm from the magnetic axis. The 4.4442 Å He-like chlorine resonance line is used in the

measurement because it has the highest intensity in the core region of the plasma. The measured line profile, which includes natural, apparatus and Doppler broadenings, is fitted with a Voigt function, from which the full half-width of the Doppler profile $\Delta\lambda_D$ is obtained. The ion temperature $T_{i,dop}$ is determined from

$$\Delta\lambda_D = 2.44\ 10^{-3}\ \lambda_o\ \sqrt{T_{i,dop}\,(\mathrm{keV}) / M\,(\mathrm{a.u.})}\ ,$$

where λ_o is the wavelength of the resonance line and M the atomic weight of the observed element.

The central ion temperatures $T_{i,dop}$ are compared with those obtained by the charge exchange method, $T_{i,ch}$. The comparison shows good agreement between the two methods. The difference between $T_{i,dop}$ and $T_{i,ch}$ is ~0.15 keV at $\bar{n}_e = 1.4 \cdot 10^{13}$ cm^{-3} and ~0.1 keV for twice this density. At still higher densities, the difference is less than 0.05 keV. Figure 10 shows the time histories of $T_{i,dop}$, $T_{i,ch}$, and the electron temperature T_e for an ohmic discharge. The central electron density n_e is measured by laser Thomson scattering ($\bar{n}_e = 5.6 \cdot 10^{13}$ cm^{-3}).

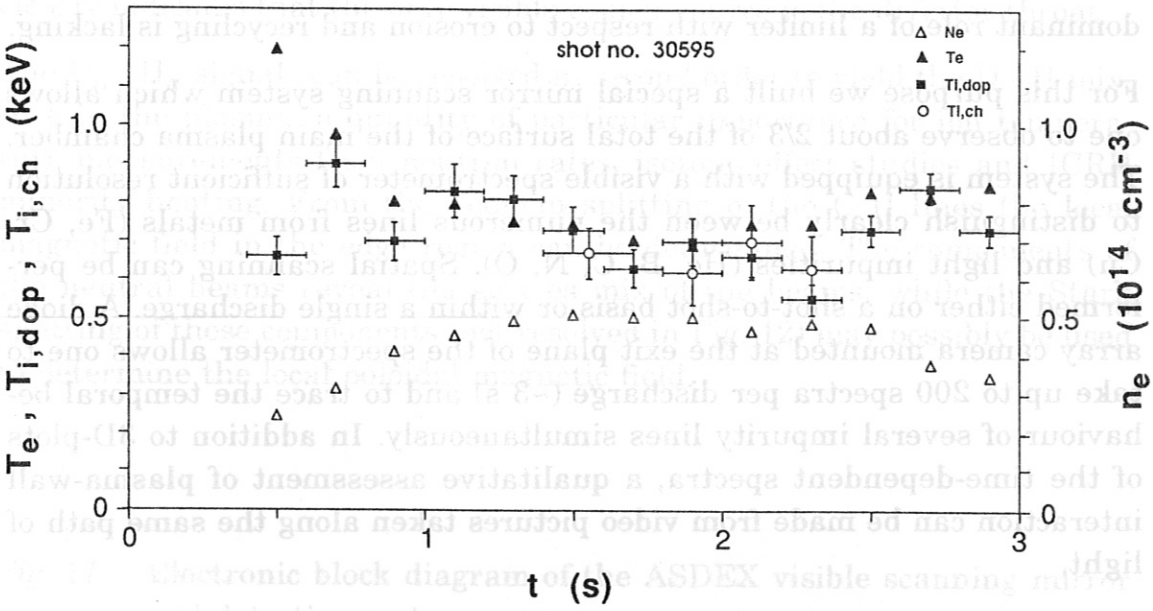

Fig. 10: Time histories of $T_{i,dop}$, the ion temperature obtained by Doppler broadening, $T_{i,ch}$, by charge exchange, T_e and n_e, the electron temperature and density obtained by laser Thomson scattering (# 30595, $B_t = 2.17$ T, $I_p = 420$ kA, $\bar{n}_e = 5.6 \cdot 10^{13}$ cm^{-3}, r = 0 cm).

The main experimental errors are due to: (1) Insufficient dynamic range of the detector. For count rates higher than 30 kHz, the detector shows saturation. (2) Statistical error in fitting the Voigt function to the line profile. (3) Broadening due to dielectronic satellites. The satellite line occurring on the right wing of the resonance line tends to increase the deduced ion temperature.

2.5 An Optical Scanning System for Spectroscopic Impurity Flux Investigations Inside the ASDEX Tokamak

(J.V. Hofmann)

In view of the great importance of impurities for the whole fusion programme it is highly desirable to obtain as much information as possible about the local origin and temporal dependence of the various impurity influxes into the plasma. The question of the spatial distribution of the influxes is emphasized for a divertor tokamak like ASDEX since here the dominant role of a limiter with respect to erosion and recycling is lacking.

For this purpose we built a special mirror scanning system which allows one to observe about 2/3 of the total surface of the main plasma chamber. The system is equipped with a visible spectrometer of sufficient resolution to distinguish clearly between the numerous lines from metals (Fe, Cr, Cu) and light impurities (He, B, C, N, O). Spatial scanning can be performed either on a shot-to-shot basis or within a single discharge. A diode array camera mounted at the exit plane of the spectrometer allows one to take up to 200 spectra per discharge (~3 s) and to trace the temporal behaviour of several impurity lines simultaneously. In addition to 3D-plots of the time-dependent spectra, a qualitative assessment of plasma-wall interaction can be made from video pictures taken along the same path of light.

A block diagram of our experimental set-up is shown in Fig. 11. The plasma light coming from a point P inside the tokamak is projected via a mirror (m1) through two quartz lenses (L1, L2) onto the entrance slit of a grating spectrometer (Czerny-Turner mount, 600 - 2400 grooves / mm, f = 1 m). The mechanical arrangement which holds the mirror can be radially shifted in a flexible bellows tube along the major radius of the torus. The mirror is able to rotate around this radial axis and in addition around an

axis perpendicular to it. The movement with respect to all three degrees of freedom is fully computer-controlled. The system also provides the possibility of scanning along a partial area of the tokamak one or several times during a discharge. During one discharge up to 4.5 full poloidal scans (full turns of the mirror) are possible. For each spectral readout the position of the mirror at the readout time is supplied.

As an example of three poloidal scans during a discharge we show a spectrum around λ = 6540 Å, Fig. 12. This spectral range contains the two resonance lines of copper in second order, the Balmer α-lines of deuterium and hydrogen and two carbon lines. In addition, the neutral beam components during neutral injection heating from 1.6 - 2.5 s (PNI = 1.6 MW) occur when the viewing line intersects the neutral beams during the scan. Furthermore, the C II lines as well as the D_α, H_α lines show Zeeman splitting in the magnetic field. The Cu I signals, only seen in one of several successive spectra, mark the inner divertor slit and result from the water-cooled Cu shields in the divertor throat. Since the mirror scans a poloidal cross-section of the ASDEX vessel several times during the discharge, the time axis in Fig. 12 is actually a space coordinate. The scan clearly indicates that the only visible copper source is the divertor throat.

The D_α / H_α signals can be resolved in second order to yield the D / H mixture in the plasma, a quantity of particular importance for ion temperature measurements from neutron rates, isotope effect studies and ICRH minority heating. From the Zeeman splitting of the C II lines the local magnetic field in the edge region can be determined. The components of the neutral beams reveal the species mix of the beams, while the Stark splitting of these components (not resolved in Fig. 12) may possibly be used to determine the local poloidal magnetic field.

Fig. 11: Electronic block diagram of the ASDEX visible scanning mirror and detection system.

Fig. 12: A 3D plot around λ = 6540 Å in the case of 3 poloidal scans during the discharge with additional heating by NI and LH.

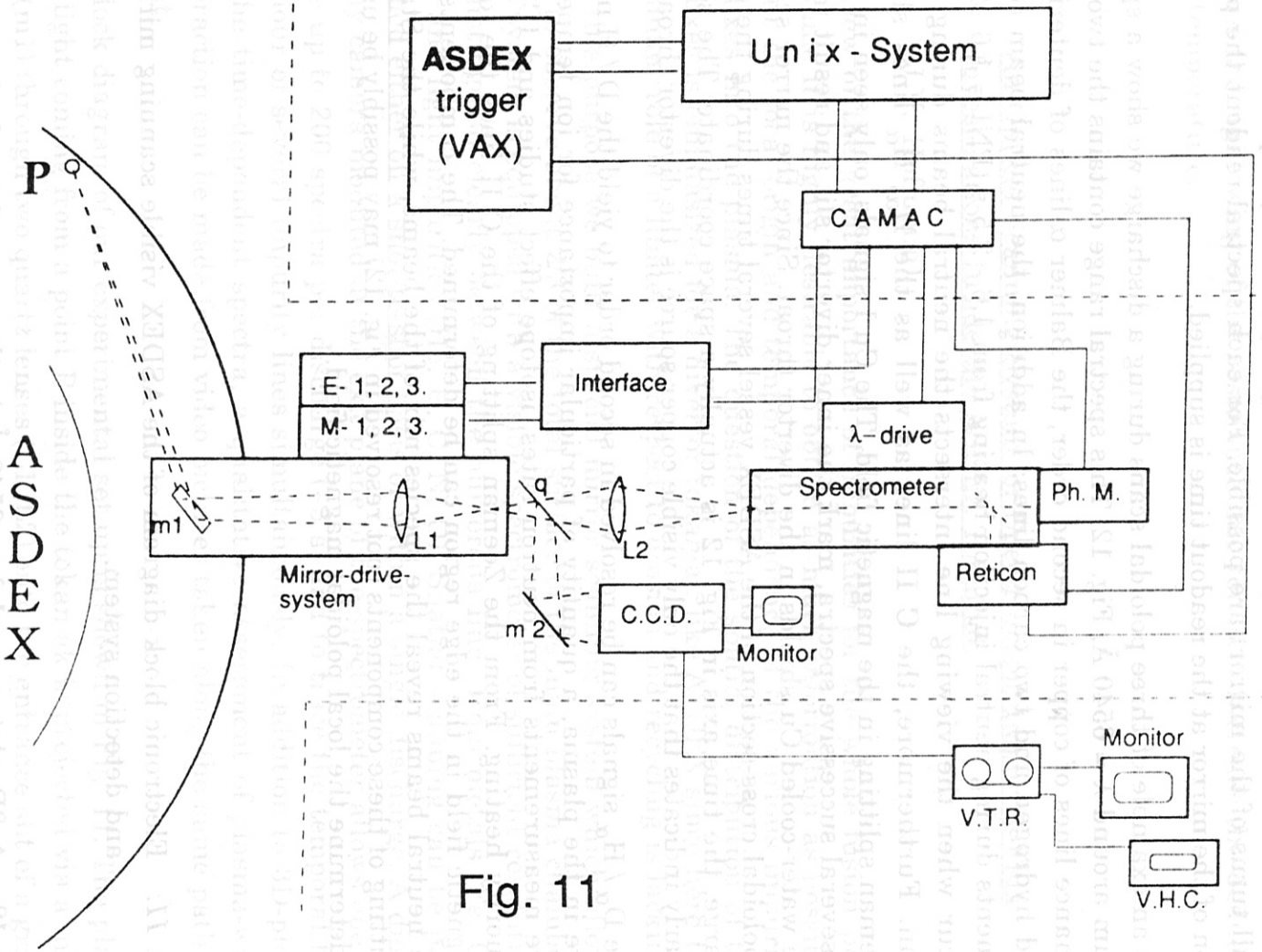
ASDEX
trigger
(VAX)
Unix - System
CAMAC
P
ASDEX
E- 1, 2, 3.
M- 1, 2, 3.
Interface
λ–drive
Spectrometer
Ph. M.
Reticon
m1
L1
q
L2
Mirror-drive-
system
m 2
C.C.D.
Monitor
Monitor
V.T.R.
V.H.C.

Fig. 11

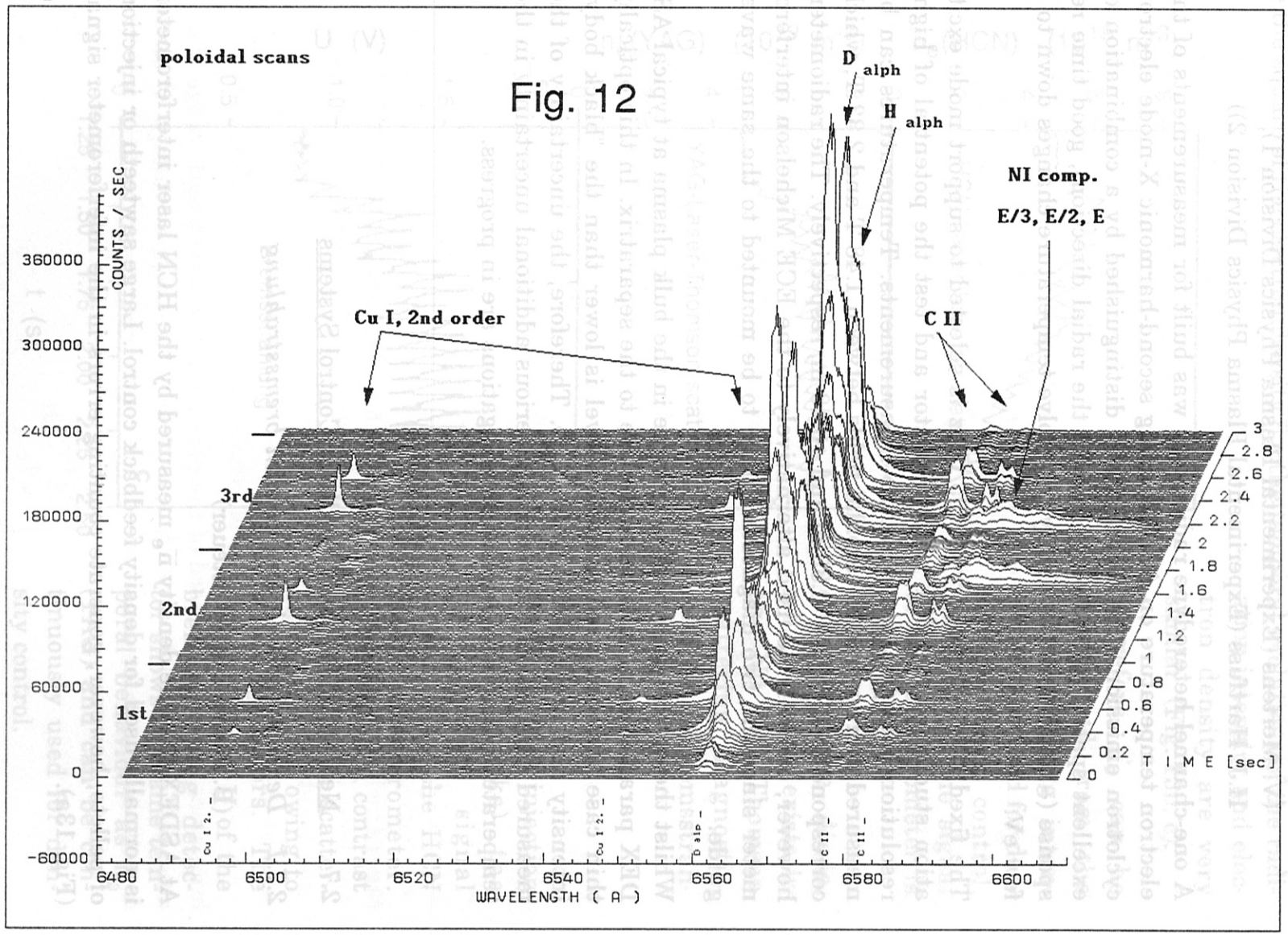
.. ASDEX V I S I B L E -SPECTROSCOPY .., LAMC: 6540 A, GR: 1200, SHOT: 28164
VBIT_3D.28164 MIRROR POS: L=165008, R=7618, S=scan, v(S)=20, iter= 7, npos 23, dtp= 20ms, dts 460 ms, 6278<S<6921
poloidal scans
Fig. 12
D alph
H alph
NI comp.
E/3, E/2, E
Cu I, 2nd order
C II
3rd
2nd
1st
COUNTS / SEC
360000
300000
240000
180000
120000
60000
0
-60000
6480
6500
6520
6540
6560
6580
6600
WAVELENGTH (A)
3
2.8
2.6
2.4
2.2
2
1.8
1.6
1.4
1.2
1
0.8
0.6
0.4
0.2
0
T I M E [sec]

2.6 High-Resolution ECE Radiometer at ASDEX

(V. Mertens (Experimental Plasma Physics Division 1),
H.J. Hartfuss (Experimental Plasma Physics Division 2))

A one-channel heterodyne radiometer was built for measurements of the electron temperature on ASDEX using second-harmonic X-mode electron cyclotron emission. The diagnostic is distinguished by a combination of excellent spatial resolution (~1 cm in the radial direction), good time response (~10 μs) and the ability to resolve temperature changes down to a few eV.

The fixed single frequency of 105 GHz is selected to support mode excitation studies of the ECE polychromator and test the potential of high-resolution boundary temperature measurements. Temperatures can be measured overlap-free at toroidal fields between 1.48 T and 2.33 T, which correspond to R_{minor} ~ -0.35 m and +0.40 m, respectively. The radiometer, however, can only be used alternatively to the ECE Michelson interferometer since the two diagnostics have to be mounted to the same waveguide.

Whilst the optical thickness τ_2^X is large in the bulk plasma at typical ASDEX parameters, τ_2^X falls below 1 close to the separatrix. In this optically thin case the measured radiation level is lower than the "black body" intensity and proportional to ($n_e T_e^2$). Therefore, the uncertainty of the measured edge density introduces a serious additional uncertainty in the temperature analysis. Detailed investigations are in progress.

2.7 New Online Density Feedback Control Systems

2.7.1 Density feedback control with bremsstrahlung

(B. Kurzan, K.-H. Steuer)

At ASDEX the line density $\bar{n}_e$ measured by the HCN laser interferometer is normally used for density feedback control. Large sawteeth or injection of pellets, however, generate counting errors in the inferferometer signal (Fig. 13a).

Since the emission coefficient of plasma bremsstrahlung is proportional to the square of the electron density $\overline{n}_e$, the temporal evolutions of the radiation intensity and electron density are very similar (Fig. 13b, c).

Therefore, $\overline{n}_e$ can be determined from the bremsstrahlung intensity and be used for density feedback control, especially if the signal of the interferometer is disturbed.

An avalanche diode, which already exists in the Nd:YAG Thomson scattering diagnostic, collects the bremsstrah-

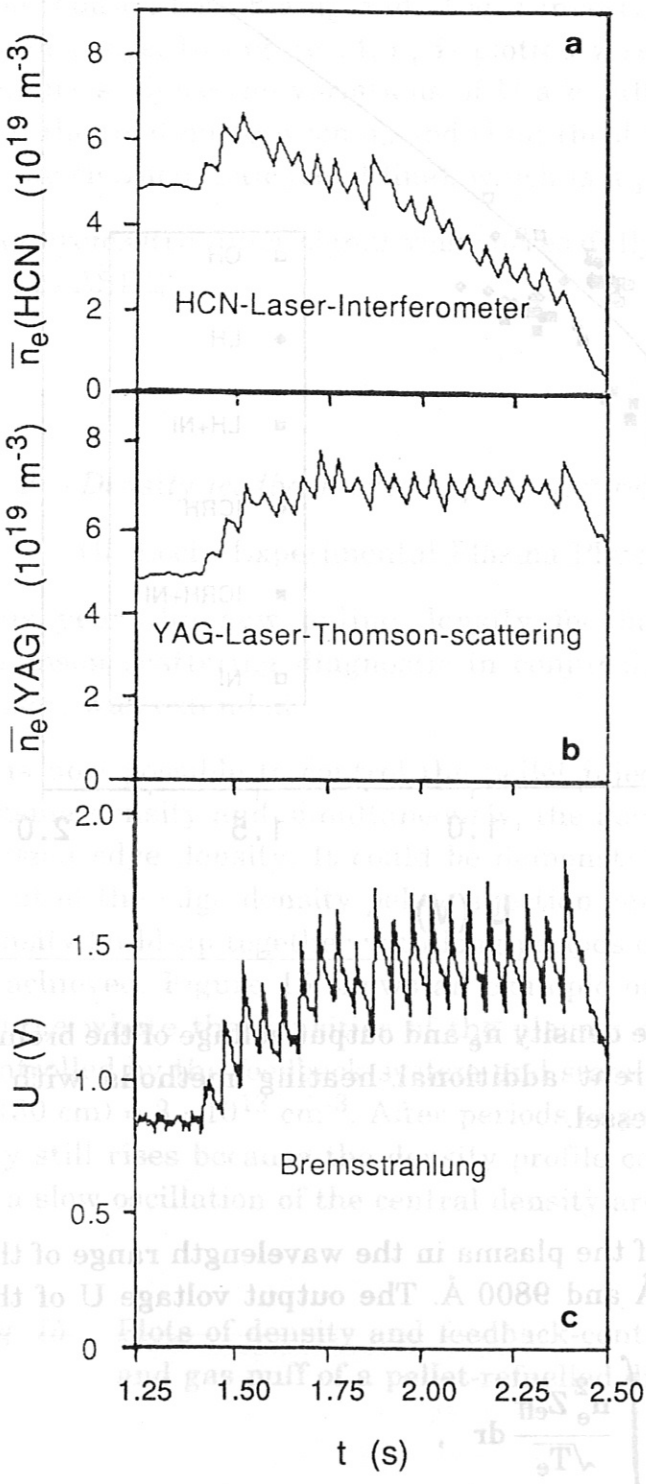

Fig. 13:
During pellet injection (density peaks) the line density signal measured by the HCN laser interferometer. (a) decreases in contrast to the Thomson scattering results. (b) owing to counting errors. The output voltage U of the bremsstrahlung detector shows the same temporal behaviour as $\overline{n}_e$ (YAG) and can be continuously used for density control.

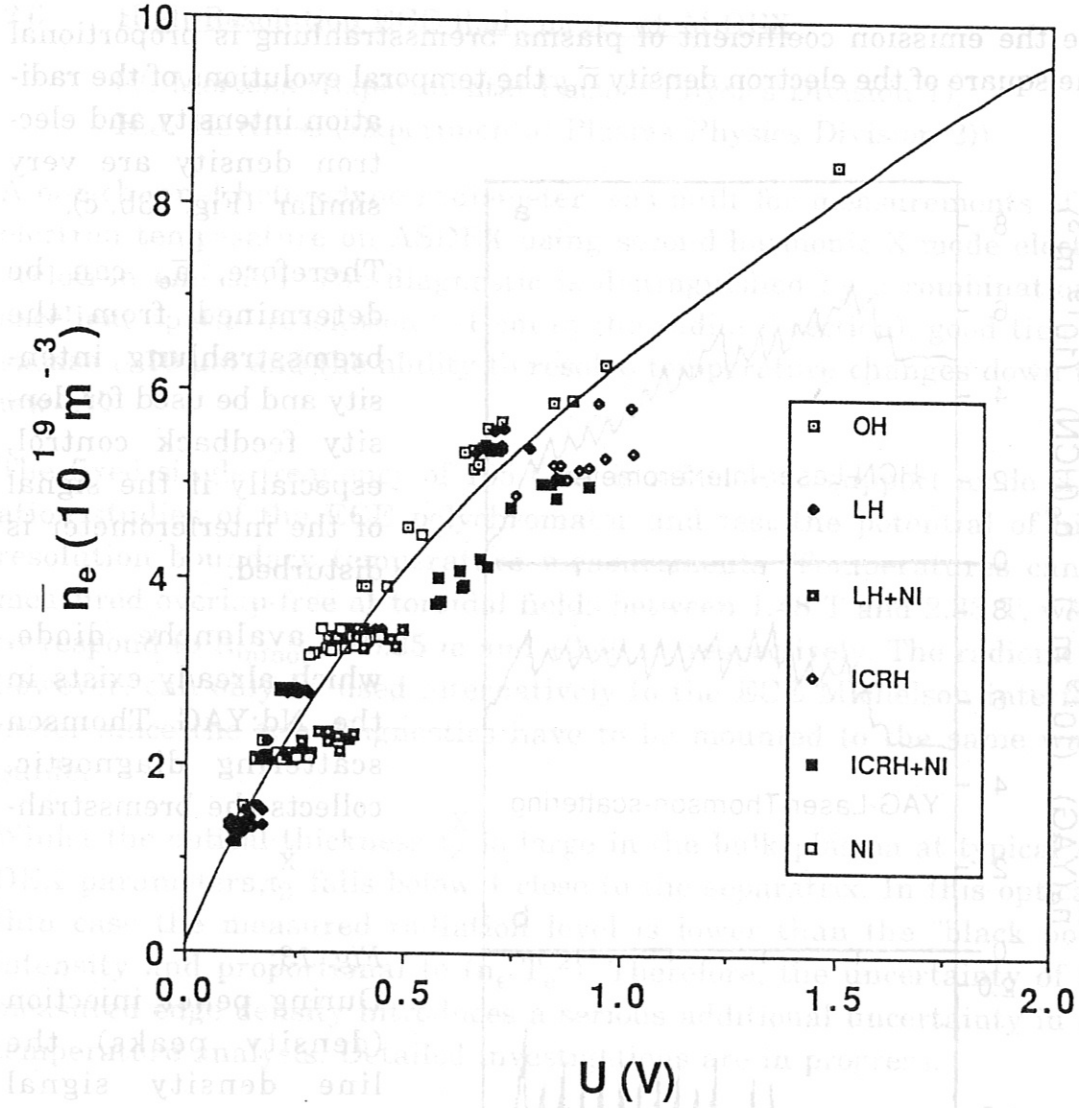

Fig. 14: Relation between line density $\bar{n}_e$ and output voltage of the bremsstrahlung for different additional heating methods with a boronized vacuum vessel.

lung along the central chord of the plasma in the wavelength range of the near infrared between 8000 Å and 9800 Å. The output voltage U of the detector is proportional to

$$\int \frac{n_e^2 Z_{eff}}{\sqrt{T_e}} \, dr \quad ,$$

with Z_{eff} as the effective ion charge and T_e as the electron temperature. Although Z_{eff} and T_e depend on the kind and power of the additional heating, the density dominates the bremsstrahlung emission.

The relation between $\overline{n}_e$ and U was investigated in a wide plasma parameter range. In Figure 14, $\overline{n}_e$ is plotted versus U for the different heating scenarios. Since the variations of U are sufficiently small, one can represent the relation between $\overline{n}_e$ and U for the different heating methods by only one characteristic (solid line), which is a polynomial fit of fourth order.

The bremsstrahlung signal was successfully used for online density control in ASDEX.

2.7.2 *Density feedback system for pellet-refuelled discharges*

(R. Loch (Experimental Plasma Physics Division 1))

This year the new online density feedback system, which uses the Thomson scattering diagnostic in conjunction with a fast CAMAC processor, was extended.

It is now possible to control the pellet injection by means of the central plasma density and simultaneously, the gas puffing rate by means of the plasma edge density. It could be demonstrated that with proper adjustment of the edge density pellet injection can be optimized and successful density build-up together with long periods of good confinement properties is achieved. Figure 15 shows an example of a pellet-refuelled ohmic discharge where the densities of the plasma centre and plasma edge were controlled by the feedback system and stabilized to $n_{eo} = 8 \cdot 10^{13}$ cm^{-3} and $n_e(30\text{ cm}) = 3 \cdot 10^{13}$ cm^{-3}. After periods of pellet injection the central density still rises because the density profile continues to peak. This results in a slow oscillation of the central density around the threshold.

Fig. 15: Plots of density and feedback-control signals for pellet injection and gas puff of a pellet-refuelled discharge.

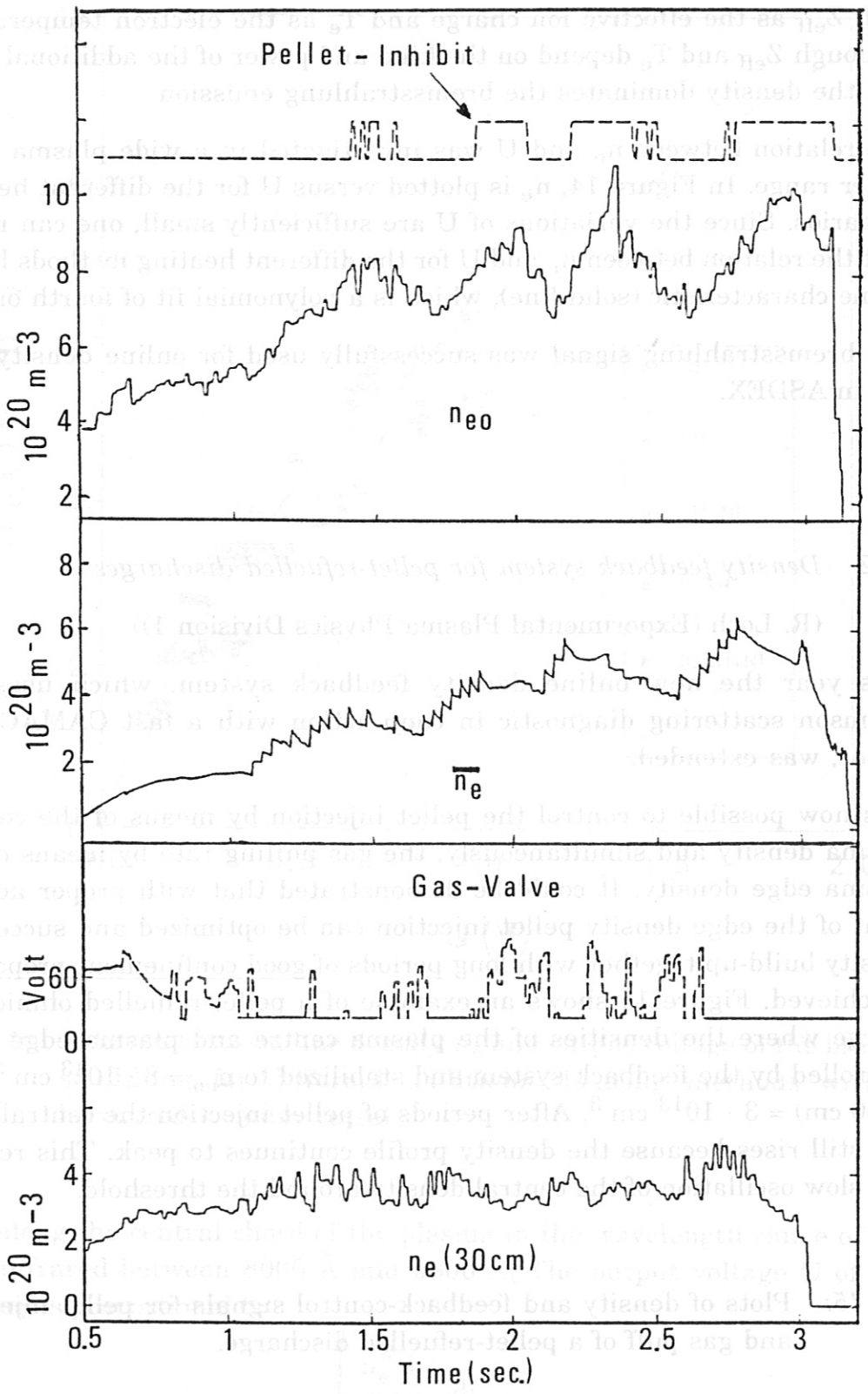
Pellet-Inhibit
10
8
6
4
2
10^{20} m^{-3}
n_{eo}
8
6
4
2
10^{20} m^{-3}
$\overline{n_e}$
Gas-Valve
Volt
60
0
4
2
0
10^{20} m^{-3}
n_e(30cm)
0.5
1
1.5
2
2.5
3
Time(sec.)

Fig. 15

2.8 Spectrally Resolved Plasma Radiation Measurements in the Near Infrared for Z_{eff} Determination

(M. Engelhard, K.-H. Steuer)

The ASDEX Thomson scattering apparatus measures the scattered light of a laser beam (λ = 1064 nm) to obtain density and temperature profiles. Furthermore, this system can be used to analyze plasma radiation in the near infrared for determining radial Z_{eff} profiles.

This method provides correct results if the measured plasma radiation consists almost completely of bremsstrahlung. But, in addition to bremsstrahlung, the plasma emits recombination and line radiation. As shown by theoretical deliberations, recombination radiation is negligible in the observed wavelength range, but line radiation cannot be excluded.

Therefore, a spectrally resolved measurement of the plasma radiation between 820 nm and 1060 nm was performed, which made it possible to identify those spectral channels of the Thomson scattering device which are not influenced by line radiation (Fig. 16).

The line-free radiation profile, together with n_e,T_e from the Thomson scattering, is used to determine Z_{eff}. The statistical errors are less then

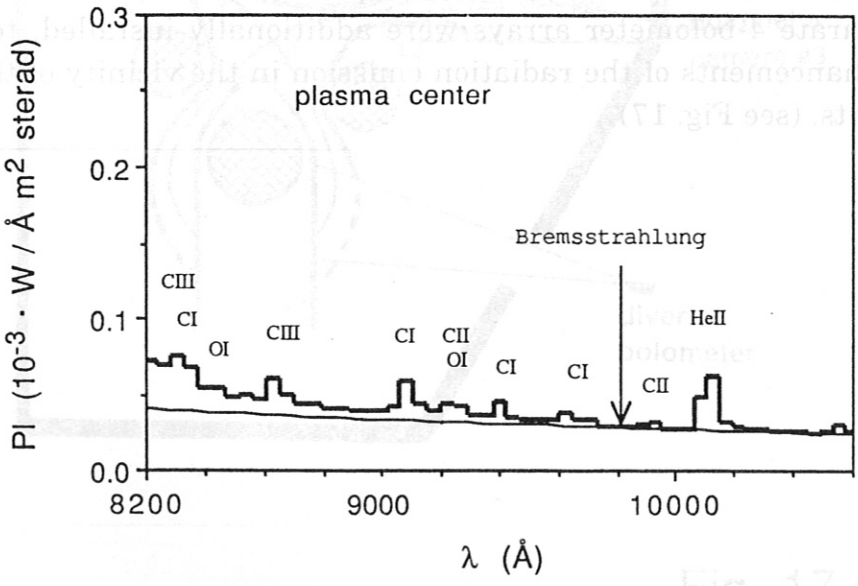

Fig. 16: The measured spectrum of plasma radiation in the near infrared, which is used for Z_{eff} determination.

10% in the plasma centre. Z_{eff} profiles obtained by bremsstrahlung and charge exchange recombination spectroscopy are in very good agreement.

2.9 Bolometric Tomography

(Th. Hartinger, E.R. Müller, R. Büchse)

Radiation asymmetries are observed close to the density limit of plasma discharges (Marfes) or at the transition from poor to improved confinement (L → H mode, SOC → IOC regime). To investigate such two-dimensional asymmetries of plasma radiation in ASDEX, it is not sufficient just to measure radial chord intensity profiles in the poloidal plane with the already existing array of 19 bolometers arranged in one horizontally viewing pinhole camera. Therefore, a second bolometer array with 16 viewing-chords in the vertical direction was installed in ASDEX. Owing to restricted port access, it was necessary to miniaturize the goldon-kapton (polyimide) film bolometer. Two-dimensional distributions of local radiation emission are obtained from the measured chord intensity profiles by means of computer tomography, and they are attributed to m = 0, 1 and 2 asymmetries. The tomography code originally developed for soft X-ray diagnostics was modified to meet the requirements of bolometry. Recently, two separate 4-bolometer arrays were additionally installed, to measure local enhancements of the radiation emission in the vicinity of the stagnation points. (see Fig. 17)

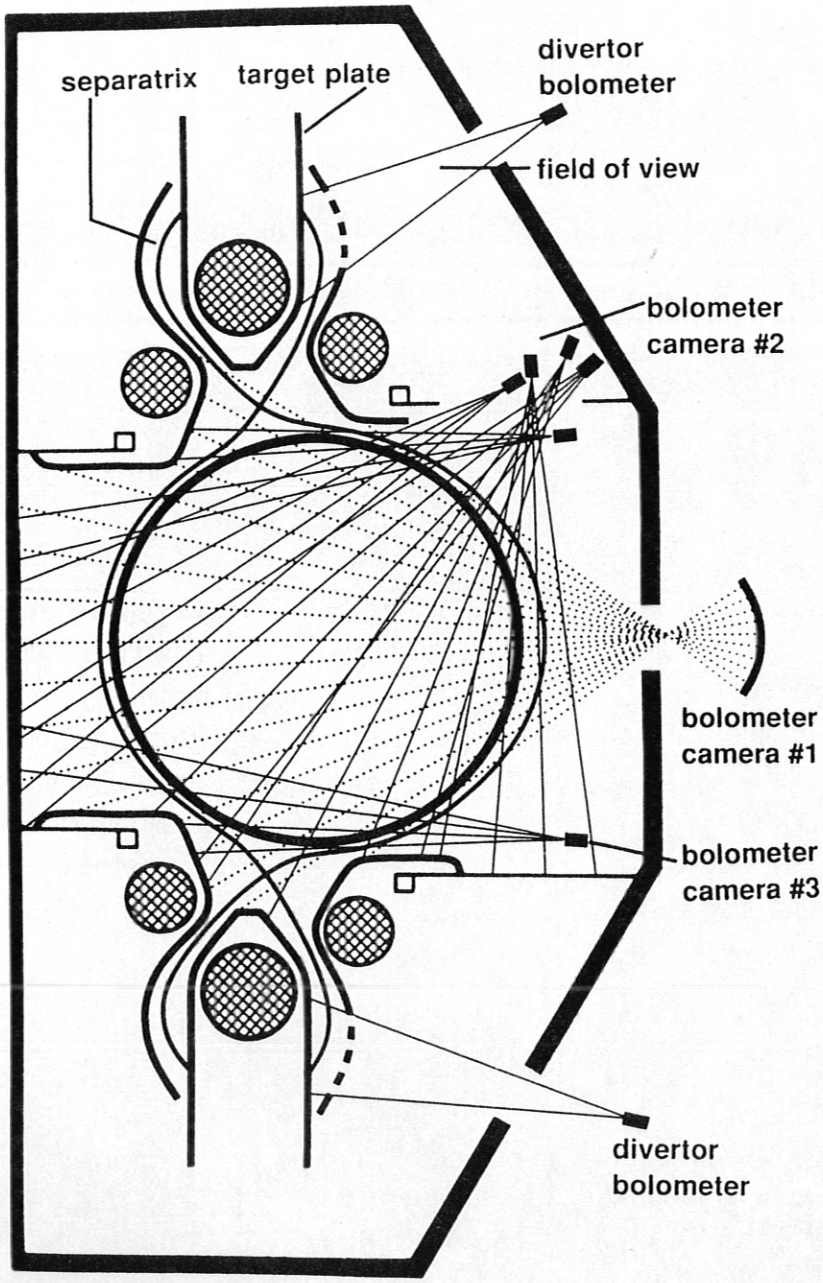
separatrix
target plate
divertor
bolometer
field of view
bolometer
camera #2
bolometer
camera #1
bolometer
camera #3
divertor
bolometer

Fig. 17